



Prediction and optimization of radiative thermal properties of nano TiO₂ assembled fibrous insulations



Jianming Yang^a, Huijun Wu^{a,*}, Moran Wang^b, Yuying Liang^a

^a School of Civil Engineering, Guangzhou University, Guangzhou 510006, China

^b Department of Engineering Mechanics, Tsinghua University, Beijing 100084, China

ARTICLE INFO

Article history:

Received 23 May 2017

Received in revised form 30 August 2017

Accepted 18 September 2017

Keywords:

Thermal insulations

Radiative thermal properties

Fibrous insulations

Nano TiO₂

Optimization

ABSTRACT

Nano titanium dioxide (TiO₂) with excellent capabilities of refraction and absorption has been acknowledged as an efficient enhancer of radiative thermal insulation performance of fibrous materials. Based on the layer-by-layer (LBL) assembling technique, nano TiO₂ was successfully assembled on the fibre surface of fibrous insulations to form nano TiO₂ assembled fibrous insulations. To obtain quantitative predictions of radiative thermal insulation enhancement of nano TiO₂ on fibrous insulations, numerical methods of radiative thermal properties were presented by combining the Rosseland equation, precise Mie theory and subtractive Kramers-Kronig relation. For validation purposes, we fabricated samples with different loading levels of nano TiO₂ and observed good agreement of radiative thermal conductivity between the measurements and our predictions. The fundamental parameters of the numerical method, including fibre diameter, loading level of nano TiO₂ and infrared transmittances, were experimentally measured through scanning electron microscopy (SEM), thermogravimetric (TG) analysis and Fourier transform infrared (FTIR) spectroscopy, respectively. The influence of loading nano TiO₂ was analysed, which presented an almost 43% reduction of the radiative thermal conductivity when the loading level of nano TiO₂ was 5.7 wt.%. The effect of fibre diameter on radiative thermal properties was also investigated to minimize the radiative thermal conductivity. A further 6% reduction of radiative thermal conductivity was predicted by optimizing the fibre diameter. The optimal fibre diameter was decreased from 1.7–2.0 μm for pure fibrous insulations to 0.9–1.0 μm for nano TiO₂ assembled fibrous insulations, which fell within the nanometre scale and could be implemented by using electrospinning technique in experiment. The methods of loading nano TiO₂ and optimizing the diameter of fibrous insulations demonstrated in this paper could serve as very useful references for enhancing radiative thermal performance and reducing heat loss in practical engineering applications.

© 2017 Elsevier Ltd. All rights reserved.

1. Introduction

Fibrous insulations with high porosity and nano or micro structure (diameter of 10 nm–10 μm) [1–3] have drawn growing attention due to their excellent mechanical properties and shielding heat conduction performance [4–7]. One promising usage of fibrous insulations is acting as fillers in composite materials [8] to improve thermal insulations, such as high performance thermal insulators [9] and vacuum insulation panels [10] in industrial and construction areas. However, radiative thermal flux may be significant as fibrous insulations are used at high temperatures [11]. To block high-temperature radiation and thereby reduce the total heat flow, nano opacifiers with excellent capabilities of refraction

and absorption, such as titanium dioxide (TiO₂) [12], carbon (C) [13], and silicon carbide (SiC) [14], are generally loaded on the fibre surfaces of fibrous insulations.

Considerable research efforts have been devoted to blocking the radiation of fibrous materials through loading nano TiO₂ on the fibre surfaces of fibrous insulations [15]. Zhao et al. [16] investigated extinction capacity enhancement of nylon 6 fibrous insulations with and without nano TiO₂. The results indicated that the extinction coefficient of TiO₂ assembled nylon 6 fibrous insulations can be increased to 220 cm⁻¹, which is much greater than that of pure nylon 6 fibrous membrane (25 cm⁻¹). Wu et al. [17] experimentally studied the thermal radiative properties of fibrous PVA (polyvinyl alcohol) films with and without nano TiO₂. The results indicated that the loading of nano TiO₂ could decrease the radiative thermal conductivity of the PVA fibrous materials by almost 30%. Zu et al. [18] experimentally measured the thermal conductivity

* Corresponding author.

E-mail address: wuhuijun@tsinghua.org.cn (H. Wu).

of an Al₂O₃ aerogel/mullite fibre composite. They found that the introduction of nano TiO₂ can significantly decrease the thermal conductivity from 0.13 to 0.058 W·m⁻¹·K⁻¹ at 800 °C and from 0.21 to 0.11 W·m⁻¹·K⁻¹ at 1200 °C.

These above experimental investigations used the experimental method to obtain the thermal radiative properties of nano TiO₂ assembled fibrous insulations. However, it is very difficult or extremely time-consuming to experimentally measure the thermal radiative properties of fibrous insulations under various conditions (e.g., different fibre diameters or different working temperatures) [19]. Therefore, efforts on exploring an effective theoretical method are needed to predict and optimize the thermal insulation performances of nano TiO₂ assembled fibrous insulations.

It is extremely difficult for commonly used theoretical methods to calculate radiative thermal properties due to the uncertain surfaces of nano TiO₂ assembled fibres. Nano TiO₂ with diameters of several nanometres assembled on the fibre surface (~1 µm in diameter) is stochastically distributed with high porosity (nearly 80%). One feasible approach is to first address the optical properties (e.g., optical constant or emissivity) [20] of given TiO₂ loading levels, thereby serving as the fundamental parameters to predict the radiative thermal properties. Unlike the smooth surfaces of pure fibres, nano TiO₂ assembled ones are composite fibres and exhibit rough surface (viz., nanolayer) with a nano porous structure, as shown in Fig. 1. This derives two other key parameters, i.e., loading level and porosity of nano TiO₂, which influence the optical and thermo-physical properties of fibrous insulations. Considering that the porosity is increased with the increase in the loading level under the experimental assembling process, a single-valued function relation between loading level and porosity is assumed, even for various fibre diameters.

The fibre diameter plays a key role in influencing the thermal radiative properties of fibrous insulations, and an optimal diameter exists for the best radiative blocking properties [21–23]. Tong and Tien [24] studied the effect of fibre diameter on the radiative thermal conductivity of silicate fibrous materials based on a two-flux analytical model. A minimum radiative thermal conductivity was found at the optimal diameters of 2.8 and 3.2 µm for pure silica fibre and silicate fibre, respectively. Arambakam et al. [25] analysed the effect of fibre diameter on radiative heat transfer through fibrous insulations based on transmittance results and used a Discrete Ordinate Method (DOM). They found that 3–10 µm was the optimal diameter of glass fibre for minimal radiation heat transfer in the temperature range of 340–750 K. They then investigated the influences on effective thermal conductivity of fibrous materials by establishing a simulation methodology [26], which predicted optimal fibre diameter for best heat insulation is about 5 µm for mineral wool fibres and 7 µm for glass fibres at 300 K.

In our previous study [3] the modelling of optical constants and radiative properties of fibrous insulations were presented by combining experimental transmittances, Mie theory [27], subtractive

Kramers-Kronig relation [28] and radiation theory [29]. The results indicated that the optimal diameters of Poly(vinylidene fluoride) (PVDF) insulations were 1.7–2.0 µm, and approximately 25% decrease of radiative thermal conductivities could be obtained by regulating the fibre diameter to the optimized value.

It can be concluded that the previous researches mainly concentrated on predicting the optimal fibre diameter for the minimum thermal conductivity of porous insulations by using the modelling. However, the predicted fibre with optimal diameter may be not implemented in experiments owing to the preparation technology of materials. For instance, the predicted optimal diameter of silica fibrous insulations was 2.8 µm [30], which was beyond the range of the existing silica fibres (i.e. 5–20 µm). Similarly, the predicted optimal diameter of PVDF fibrous insulations was 2.0 µm in Ref. [3], which was also beyond the range of the existing electrospun PVDF fibres (i.e. 0.2–1.0 µm). Therefore, regulating the optimal fibre diameter for the minimum thermal conductivity has current significance for obtaining the ideal fibres in experiment. Assembling nanoparticles onto the fibre surface seems to be a feasible method, as this not only improves the radiation insulation but also alters the spectral optical constants. The thermal radiative properties of composite fibres could be modified and regulated by the nanoparticle coating, which provides a possible way to regulate the optimal fibre diameter to fit the existing materials in experiment.

The previous researches on the optimal diameter for the minimum thermal conductivity mainly were conducted concerning a single type of fibres. When it comes to composite fibres (e.g. fibres loading nanoparticles), there are very limited reported studies. In this communication so as to further block the radiative flux and thereby improve the thermal insulation of PVDF fibrous insulations, the surface of PVDF fibres was assembled with a porous layer of nano TiO₂. The modelling for the optical constants and radiative properties of the composited TiO₂/PVDF fibres was presented. The optimal fibre diameter was predicted and also feasible for the existing materials in experiment by regulating the loading level of TiO₂ nanoparticles.

2. Numerical methods

2.1. Thermal radiation models

Nano TiO₂ assembled fibrous insulations with excellent capabilities of refraction and absorption are extremely optically thick media when used as thermal insulating materials. In this situation, radiative heat transfer can be modelled based on the Fourier law of heat conduction, which is called the diffusion approximation method, as determined by the Rosseland equation [29,31]

$$k_r = \frac{16n_T^2\sigma T^3}{3\beta_{eT}} \quad (1)$$

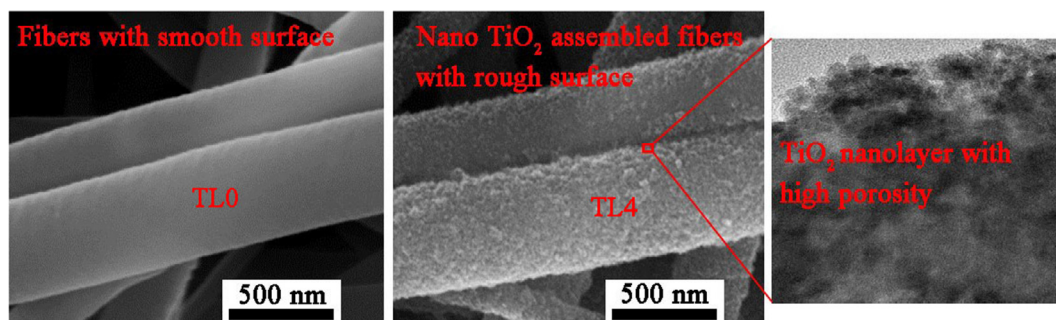


Fig. 1. Comparison of surface morphologies of fibres and nano TiO₂ assembled ones.

where T is the temperature, $\sigma = 5.67 \times 10^{-8} \text{ W}\cdot\text{m}^{-2}\cdot\text{K}^{-4}$ is the Stefan-Boltzmann constant, and n_T is the temperature-dependent effective refractive index, which can be calculated as follows [32]

$$n_T = \left(\int_0^\infty \frac{1}{n_{c\lambda}} \frac{\partial E_{b\lambda}}{\partial E_b} d\lambda \right)^{-1} \quad (2)$$

where $n_{c\lambda}$ is the spectral refractive index of the composite, which can be approximately calculated by $n_{c\lambda} = \sum_{i=1}^m n_{i\lambda} v_i$, where $n_{i\lambda}$ is the spectral refractive index of component i (e.g. composite nanofibres or air), concerning to the air within the composite n_i equals to 1, v_i is the volume fraction of component i . $E_{b\lambda}$ is the spectral black-body emissive power calculated by Planck's law, and E_b is the black body emissive power, defined as [29]

$$E_{b\lambda}(T, \lambda) = \frac{2\pi hc_0^2}{n_T^2 \lambda^5 [e^{hc_0/n_T \lambda kT} - 1]} \quad (3)$$

$$E_b = n_T^2 \sigma T^4 \quad (4)$$

where $h = 6.626 \times 10^{-34} \text{ m}^2\cdot\text{kg}\cdot\text{s}^{-1}$ is Planck's constant, $c_0 = 2.998 \times 10^8 \text{ m}\cdot\text{s}^{-1}$ is the light speed in a vacuum, and $k = 1.38 \times 10^{-23} \text{ J}\cdot\text{K}^{-1}$ is the Boltzmann constant.

In Eq. (1), β_{eT} is the Rosseland mean extinction coefficient, which indicates the temperature-dependent mean extinction capability, expressed as [33]

$$\beta_{eT} = \left(\int_0^\infty \frac{1}{\beta_{e\lambda}} \frac{\partial E_{b\lambda}}{\partial E_b} d\lambda \right)^{-1} \quad (5)$$

where the spectral extinction coefficient, $\beta_{e\lambda}$, represents an overall value of extinction capacity by considering the attenuation in heat flux direction while neglecting the parts of vertical directions [33]. $\beta_{e\lambda}$ can be calculated for various spectral lengths by [34]

$$\beta_{e\lambda} = \int_{\omega_{f1}}^{\omega_{f2}} \int_{\zeta_{f1}}^{\zeta_{f2}} \int_0^\infty 2r Q_{e\lambda} N(r(R_f)) dr d^2F \quad (6)$$

where d^2F and $N(r(R_f))$ are the orientation distribution and number size distribution, and the limits of integration (ω , ζ) denote the range of the angular orientation of fibres.

As PVDF fibres are infinite cylinders and vertical to the direction of the thickness, $\beta_{e\lambda}$ can be expressed as

$$\beta_{e\lambda} = 4Q_{e\lambda} v_f / \pi d \quad (7)$$

where v_f is the volume fraction, d is the fibre diameter, and $Q_{e\lambda}$ is the extinction efficiency.

2.2. Extinction efficiencies

The extinction efficiency is a non-dimensional and temperature-independent parameter indicating the capacities of absorbing and scattering light as the light goes through a fibre. Regarding composite fibres, such as nano TiO₂ assembled ones, $Q_{e\lambda}$ should be a combination of extinction efficiencies of components, viz. TiO₂ spherical nanoparticles ($Q_{e\lambda,s}$) and infinite cylindrical fibres ($Q_{e\lambda,c}$). Their scattering geometries from an incident light are shown in Fig. 2. The classic Mie scattering theory for spherical particles and cylindrical fibres [28,35] can be used to calculate $Q_{e\lambda,s}$ and $Q_{e\lambda,c}$ respectively

$$Q_{e\lambda,s} = \frac{2}{x^2} \text{Re} \left[\sum_{j=1}^\infty (2j+1)(a_j + b_j) \right] \quad (8)$$

$$Q_{e\lambda,c} = \frac{1}{x} \text{Re} \left[(a_0 + b_0) + 2 \sum_{n=1}^\infty (a_n + b_n) \right] \quad (9)$$

where Re is the symbol of real part, $x = \pi d/\lambda$ is the size factor, a_j and b_j are the Mie coefficients of a sphere, and a_n and b_n are the Mie coefficients of a cylinder. As radiation heat flux is vertically incident on spherical and cylindrical particles, these Mie coefficients can be respectively expressed as

$$a_j = \frac{[D_j(mx)/m + j/x]J_j(x) - J_{j-1}(x)}{[D_j(mx)/m + j/x]Y_j(x) - Y_{j-1}(x)} \quad (10)$$

$$b_j = \frac{[mD_j(mx) + j/x]J_j(x) - J_{j-1}(x)}{[mD_j(mx) + j/x]Y_j(x) - Y_{j-1}(x)} \quad (11)$$

$$a_n = \frac{[D_n(mx)/m + n/x]J_n(x) - J_{n-1}(x)}{[D_n(mx)/m + n/x]H_n(x) - H_{n-1}(x)} \quad (12)$$

$$b_n = \frac{[mD_n(mx) + n/x]J_n(x) - J_{n-1}(x)}{[mD_n(mx) + n/x]H_n(x) - H_{n-1}(x)} \quad (13)$$

where J_n and Y_n are the first and second kind of Ricatti-Bessel function, respectively, which are internal functions in the MATLAB software. $H_n = J_n + iY_n$ is the first kind Hankel function, D_j and D_n are the recurrence relation for computations, which is satisfied with the flowing logarithmic derivatives:

$$D_{j-1}(x) = \frac{j}{x} - \frac{1}{(j/x) + D_j(x)} \quad (14)$$

$$D_{n-1}(x) = \frac{n-1}{x} - \frac{1}{(n/x) + D_n(x)} \quad (15)$$

During the calculation of extinction efficiency, the optical constant (m) consists of the refractive index (n_i) and absorption index (κ_i) [36], which indicate the scattering and absorption capabilities of fibrous materials, respectively. Fig. 3(a) and (b) shows the extinction efficiencies of spherical TiO₂ nanoparticles and cylindrical PVDF fibres, based on Eqs. (8) and (9) respectively. The spectral optical constants of TiO₂ particles (m_s) and PVDF fibres (m_f) are referred to Ref. [36] and Ref. [3] respectively. The diameters of the spheres and the cylinders are presented as 0.01 μm and 1 μm , respectively.

It can be observed that with the increase in the wavelength, the extinction efficiencies of TiO₂ particles and PVDF fibres present a similar trend, increased firstly and then decreased with a maximum value. The maximum extinction efficiency exists at wavelength of $\sim 0.01 \mu\text{m}$ for TiO₂ particles, and $\sim 1 \mu\text{m}$ for PVDF fibres. However, the extinction efficiency of TiO₂ particles get close to zero beyond a wavelength of 0.1 μm . According to Wien's displacement law [37], the majority of the radiative flux occurs at a wavelength of $\sim 8 \mu\text{m}$ for the temperature range of 300–400 K. Therefore below a wavelength of 0.1 μm the radiative flux could be completely neglected. When the extinction efficiency of spherical particles is considered as a superimposed value by multiplying the quantity of nano TiO₂, the extinction coefficient by Eqs. (5)–(7) would be obtained with zero at 300–400 K. However, in fact the extinction coefficient of nano TiO₂ should be a value with equal magnitude when compared with that of cylindrical fibres, rather than zero. This difference may be caused by the existence of the internal scattering radiation within the porous layer of nano TiO₂, which would be considerably increasing the extinction efficiency.

Therefore, concerning to nano TiO₂ assembled fibres, the extinction efficiency is not merely a simple superimposed value. In order to precisely evaluate the extinction capacity of nano TiO₂ assembled fibres, an integrated structure of the composite fibre is assumed. Regarding the integrated structure, as shown in Fig. 1, nano TiO₂ is well assembled on the surface of cylindrical fibres with one certain loading level, thickness and porosity of TiO₂

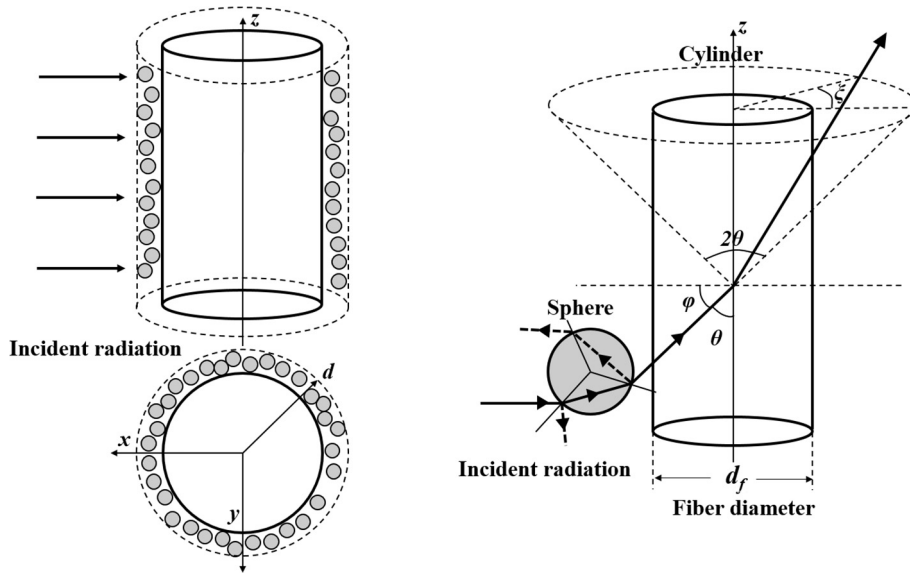


Fig. 2. Scattering geometry for nano TiO₂ assembled fibres from incident radiation.

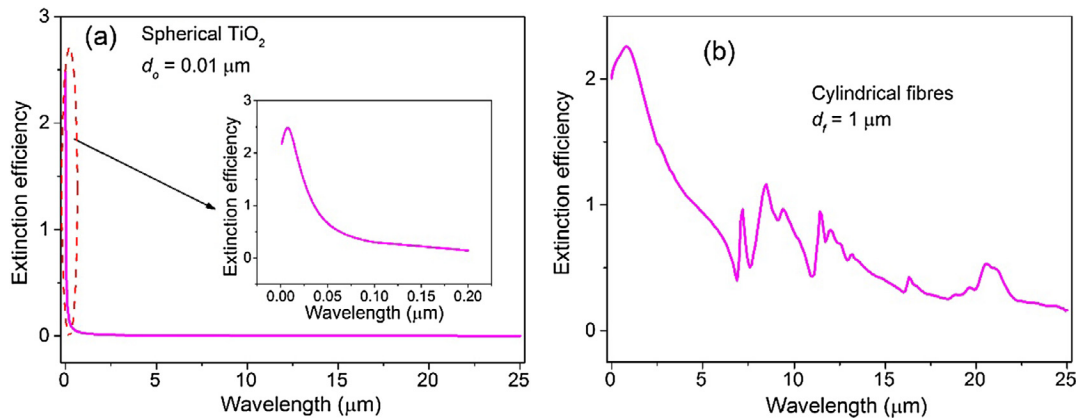


Fig. 3. Extinction efficiencies for various wavelengths. (a) Nano TiO₂, (b) fibre.

nanolayers. The numerical predictions of extinction efficiencies and radiative thermal conductivities would be based on the integrated structure by Eq. (9).

2.3. Optical constants

Based on our previous investigation of m of fibrous insulations, two calculating relations between n_λ and κ_λ indices were built to obtain unique numeric solutions of m_λ with the wavelength ranging between 2.5 and 25 μm . Ignoring internal scattering radiation between fibres and opacifiers, a relation combining the extinction coefficient and Beer's law [38] could be obtained:

$$Q_{ei} = -\frac{\pi d \ln(\tau_\lambda)}{4L v_f} \quad (16)$$

where L is the thickness, and τ_λ is the experimental spectral transmittance. Combined with Eq. (9), a relation between n_λ and κ_λ could be established.

Besides the above equation, another equation of n_λ and κ_λ can be provided by the subtractive Kramers-Kronig relation [28,38]:

$$n(\lambda) = n(\lambda_i) + \frac{2(\lambda_i^2 - \lambda^2)}{\pi} P \int_0^\infty \frac{\lambda_0 \kappa(\lambda_0)}{(\lambda^2 - \lambda_0^2)(\lambda_i^2 - \lambda_0^2)} d\lambda_0 \quad (17)$$

where λ_i is the initial wavelength. In the numerical calculation, $\lambda_i = 0.5 \mu\text{m}$, and $n(\lambda_i)$ is the initial refractive index. Regarding a composite fibre, $n(\lambda_i)$ is a combination of components by multiplying their ratios. As such, $n(\lambda_i)$ of nano TiO₂ assembled fibres can be expressed as

$$n(\lambda_i) = n_f(\lambda_i)w_o + n_o(\lambda_i)(1 - w_o) \quad (18)$$

where $n_f(\lambda_i)$ and $n_o(\lambda_i)$ are the initial refractive indices of fibre and nano TiO₂, respectively. In the numerical calculation, $n_o(\lambda_i) = 2.75$ and $n_f(\lambda_i) = 1.41$ [3]. w_o is the loading level of nano TiO₂ and can be obtained through experimental measurements.

Uniqueness analysis of optical constants is the key approach to evaluate the reliability of the numerical results. For spherical particles, Milham et al. [40] and Ruan et al. [39] performed uniqueness analysis by determining valid uniqueness regions of $0 \leq k \leq (2 + 2.4x)^{0.5}$ and $10^{-2} \leq x \leq 2$. For cylindrical fibres, we concluded that the solutions n_λ and κ_λ of PVDF fibres were unique as the diameter was less than d_c of 1.06 μm . Therefore, to ensure unique solution optical constants by using the numerical method, the fibres would be prepared by using electrospinning technology.

3. Samples and experimental procedure

In this work, PVDF fibrous insulations produced by means of electrospinning technology [3] were used as the basic material with a primary average fibre of 520 nm. Nano TiO₂ (≥99.99%, diameter ~10 nm, purchased from Xuancheng Jingrui New Material Co. Ltd., China) was assembled on the surface of the as-prepared PVDF fibres by the layer-by-layer self-assembly technique [41], as shown in Fig. 4. First, negatively charged PVDF fibrous insulation was immersed into anionic poly(acrylic acid) (PAA from Damao Co. Ltd., China) solution for 15 min and three times in pure water for 1 min each time. Second, the PAA-attached PVDF fibres were placed into cationic TiO₂ solution for 15 min and three times in pure water for 1 min each time. Finally, the two procedures were repeated until n layers of TiO₂ were assembled. Three samples of fibrous insulations with different TiO₂ layers (TL2–TL6) were prepared by regulating the assembling times (viz., 2, 4 and 6 layers, respectively).

The microstructure of the samples was measured by using a field emission scanning electron microscope (FESEM, model JSM-7001F from JEOL Co., Japan). Fig. 5(a) and (b) shows the SEM images of PVDF fibres (TL0) and nano TiO₂ assembled ones (TL2) respectively. The surface morphology of nano TiO₂ assembled fibres presented apparently rough, when compared with pure fibres with a smooth surface morphology. This rough surface was in fact a layer of porous nano TiO₂, and the porosity in this layer can be calculated by

$$\varphi = 1 - \frac{d^2 - d_i^2}{d^2} \bigg/ \frac{(m_o/m_f)(\rho_f/\rho_o)}{1/[1 - (d^2 - d_i^2)/d^2]} \quad (19)$$

where $d_i = 0.52 \mu\text{m}$ is the diameter of the pure PVDF fibre, m_o/m_f is mass ratio of nano TiO₂ to fibre, and ρ_f/ρ_o is the mass ratio of fibre to nano TiO₂.

The diameter distribution was then obtained by Nano-measurer software from 50 fibre diameters, and the average fibre diameter (d) was obtained by normal curve fitting, as shown in Fig. 5(b). The average diameters of TL2, TL4 and TL6 were 0.55, 0.58 and 0.582 μm , respectively. The diameter standard deviation of TL0 is 0.096 μm , which is greater than that of TL2–TL6, with 0.056, 0.051 and 0.058 respectively. This is because with the increase in fibre diameter, the specific surface area of the fibres decreases, which would also decrease the access to having the fibres assembled with the nano TiO₂. Therefore, after the TiO₂ assembling process, the diameters of TiO₂ assembled fibres (TL2–TL6) would get close to the average fibre diameter, which indicates a smaller standard deviation than that of pure fibres (TL0).

A thickness gauge from Chen Lu Co. Ltd., China, was used to obtain the thickness (L) of nano TiO₂ assembled fibrous insulations.

The thicknesses were 33, 35 and 34 μm for TL2, TL4 and TL6, respectively.

A thermal gravimetric analyser (TGA, model 400, PerkinElmer, U.S.) was employed to determine the composition of nano TiO₂ assembled fibrous insulations. The samples were tested at a heating rate of 10 °C/min up to 800 °C, and under a nitrogen flow rate of 50 mL/min. The TGA thermograms of TL0–TL6 is shown in Fig. 6. It can be seen that the pure PVDF fibres were completely decomposed at 800 °C, while the nano TiO₂ assembled ones were decomposed with residual. Herein, the weight percentages of the residual are the mass ratios of nano TiO₂ to composite fibres, which can be calculated by

$$w_o = \frac{m_o}{m_i} \times 100\% \quad (20)$$

where m_o is the mass of TiO₂ (i.e., the residual mass), m_i is the initial mass of composite fibres. Then the mass contents of TiO₂ (i.e., the loading levels) were obtained with 1.84, 5.30 and 5.70 wt.% for TL2, TL4 and TL6, respectively, as listed in Table 1.

A Fourier transform infrared (FTIR) spectroscopy gauge (model Tensor27 from Bruker Co., Germany) was used to test the infrared spectral transmittances (τ_λ). The testing values of transmittances were obtained by averaging two measurements at the front and reverse sides of samples [3]. The experimental deviations from the average transmittances (TL4) were shown in Fig. 7(a), which presents deviations in a range of 0.8–5.6%. Fig. 7(b) shows the average spectral transmittances of TL0–TL6 for various wavelengths of 2.5–25 μm . It can be seen that the transmittances significantly fluctuated with wavelengths. TL2–TL6 presented smaller transmittances than TL0. This is because nano TiO₂ exhibits strong absorption and scattering abilities toward radiative light. Considering a central wavelength of ~7 μm for the temperature of 400 K [37], Fig. 7(c) compares transmittances of TL4 and TL6 in a wavelength range of 6–8 μm . In these wavelengths, it seems that the average transmittances of TL6 are generally greater than that of TL4. However, it always exists a spectral transmittance that is in the scope of both TL4 and TL6 when taking experimental deviations into consideration. Therefore, the difference of transmittances between TL4 and TL6 would be insignificant.

4. Results and discussion

4.1. Validation of theoretical models of radiative thermal conductivity

Based on the spectral transmittances of nano TiO₂ assembled fibrous insulations, the optical constants (viz., absorption index and refractive index) could be numerically calculated by Eqs. (16)–(18), as shown in Fig. 8. According to optical theories, the

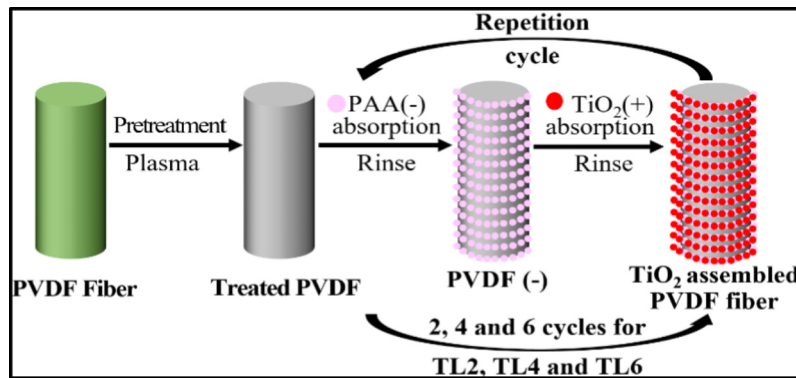


Fig. 4. Schematic of layer-by-layer self-assembly technique.

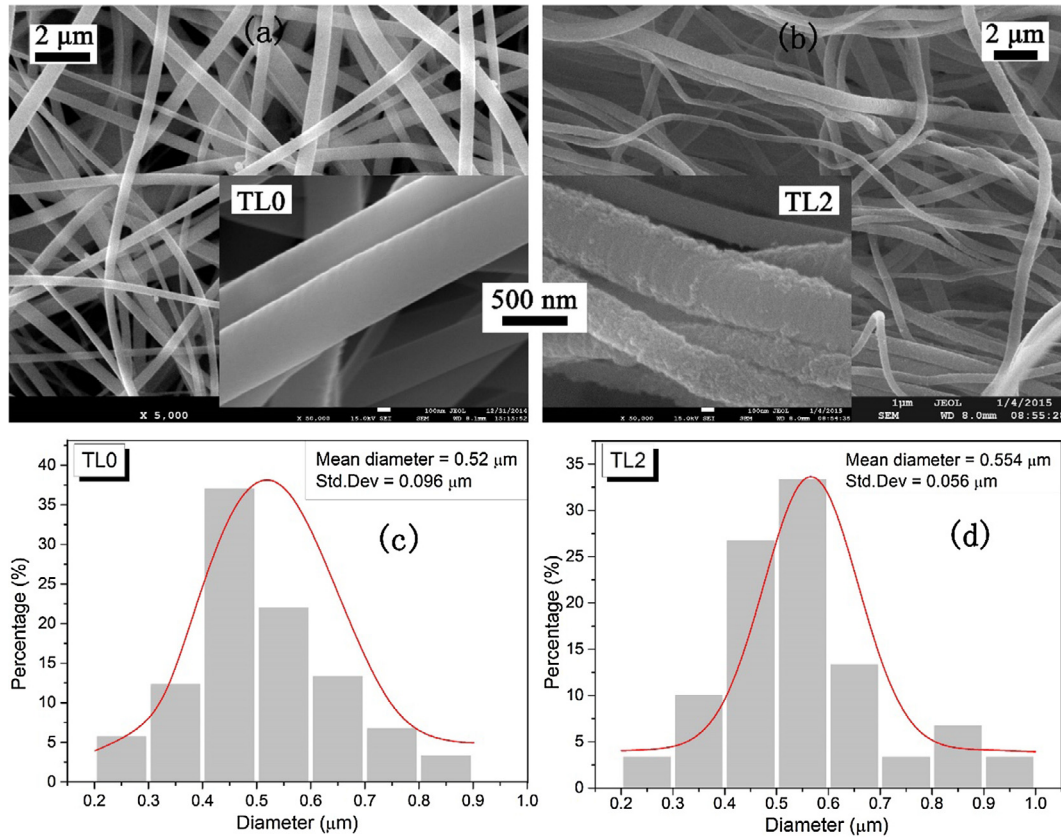


Fig. 5. (a) SEM image of fibres and (b) TiO₂ assembled ones, (c) normalized diameter distribution of fibres and (d) TiO₂ assembled ones.

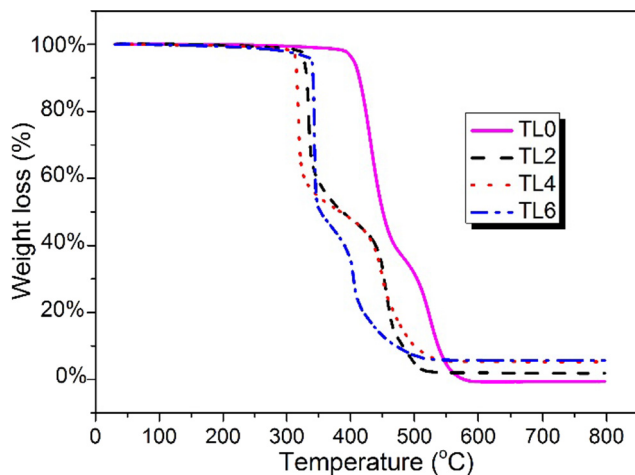


Fig. 6. TGA thermograms of fibres and TiO₂ assembled ones.

sum of the transmittance, absorption and scattering ratio is 1. This indicates that as the PVDF fibres present greater transmittance, they should show a smaller absorption index and/or refractive

index after assembling TiO₂. It is consistent with the transmittances in Fig. 7, which shows TL0 has a smaller optical constant as it presents a greater transmittance.

Based on the measured transmittances and Beer's Law, the experimental extinction efficiency could be calculated from Eq. (16), and radiative thermal conductivity could be respectively expressed as

$$k_{r,\tau} = \frac{16\sigma n_i^2 T^3}{3\beta_{eT,\tau}} \quad (21)$$

where $\beta_{eT,\tau}$ is the experimental mean extinction coefficient

$$\beta_{eT,\tau} = \left(\int_0^\infty \frac{1}{\beta_{e\lambda,\tau}} \frac{\partial E_{b\lambda}}{\partial E_b} d\lambda \right)^{-1} \quad (22)$$

where $\beta_{e\lambda,\tau}$ is the experimental spectral extinction coefficient, which can be calculated by Eq. (7).

Fig. 9(a) and (b) compares the numerical radiative thermal conductivities of TL0–TL6 from the present model and experimental data at 300 and 400 K. The properties used in the simulations include the diameter, thickness, and volume fraction of TL0–TL6. The present predictions of TL0 are slightly lower (nearly 2%) than the experimental data, which may be due to the diversity of experimental diameters as the diameter is averaged in the simulations.

Table 1
Structural properties of nano TiO₂ assembled fibrous insulations.

Samples	Average diameter (µm)	Std. Dev of diameter (µm)	Loading level of TiO ₂ (%)	Thickness (µm)	Volume fraction of fibres (%)	Porosity of TiO ₂ (%)
TL0	0.520	0.096	–	36	3.00	–
TL2	0.554	0.056	1.84	33	3.02	90.3
TL4	0.580	0.051	5.30	35	3.09	84.0
TL6	0.582	0.058	5.70	34	3.10	83.3

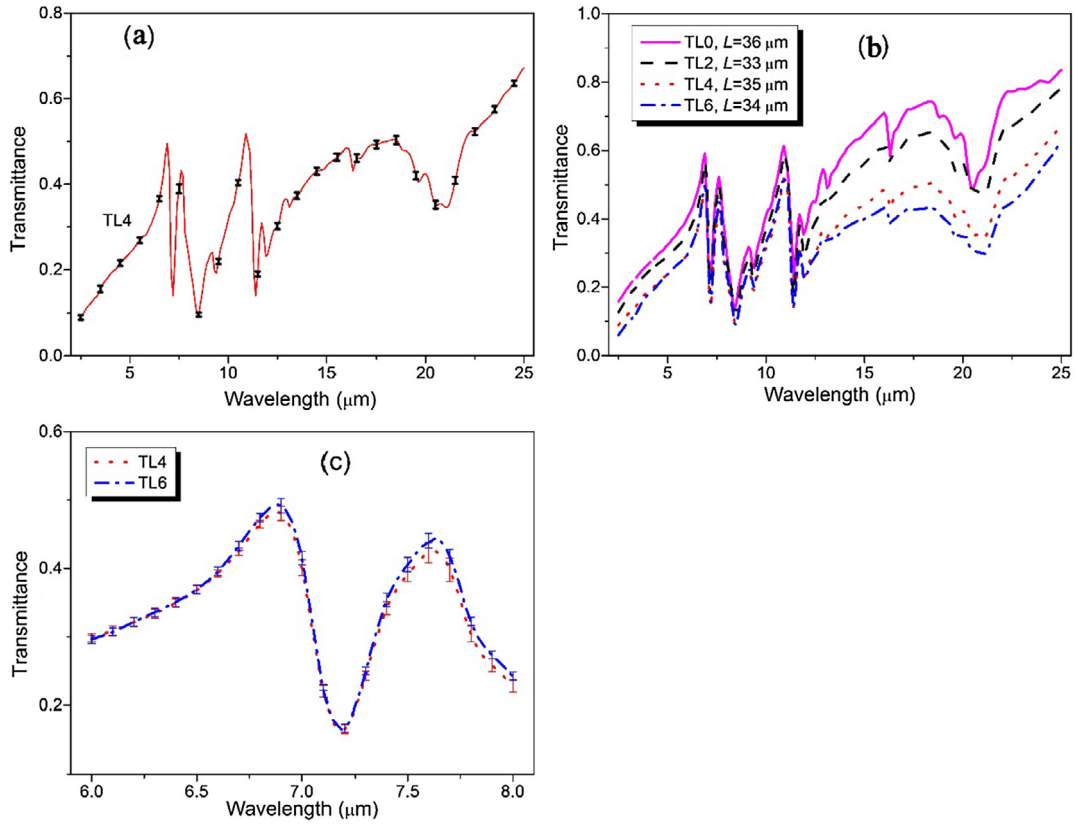


Fig. 7. Measured spectral transmittances for various wavelengths. (a) Example (TL4) of transmittances with deviations, (b) transmittances of TL0–TL6 in 2.5–25 μm, (c) comparisons of transmittances between TL4 and TL6 in 6.0–8.0 μm.

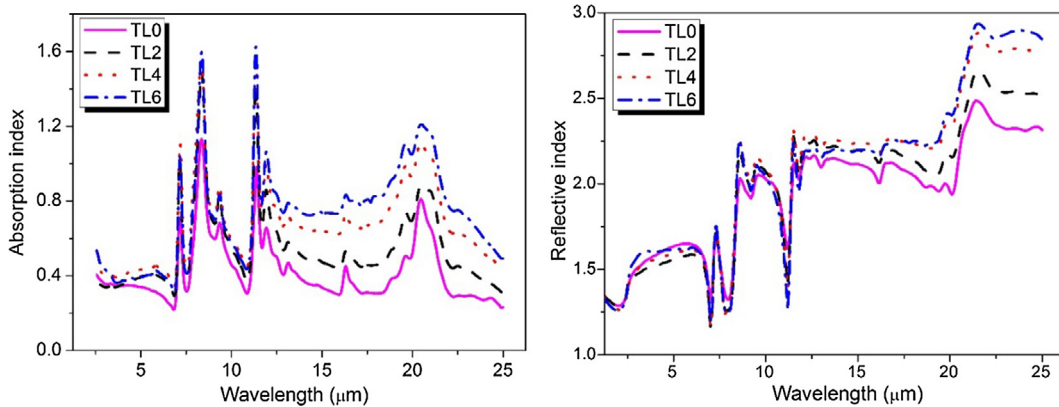


Fig. 8. Predicted optical constants for various wavelengths.

Note that the calculated results of radiative thermal conductivities of TL2–TL6 agree well with the experimental ones, which shows smaller difference than that of TL0. It may be caused by the smaller standard deviations of TL2–TL6 (i.e. 0.056, 0.051 and 0.058 μm respectively) than that of TL0 (i.e. 0.096 μm). Although the uncertainty of TiO₂ diameter would also influence the difference between numerical and experimental results, this influence should be less significant than that caused by the diameter deviation of composite fibres.

Fig. 9(b) shows that the radiative thermal conductivity at 400 K presents a slight increase (only 0.93%) from TL4 to TL6. This is consistent with the comparison of transmittances in Fig. 7(c), which

indicates that the transmittances of TL6 are slightly greater than that of TL4. Note that the 0.93% difference of the radiative thermal conductivity between TL4 and TL6 is smaller than the experimental deviations of both TL4 (2.0%) and TL6 (1.6%). Therefore, it is reasonable to assume that TL4 and TL6 have approximately equal radiative thermal conductivities, although an average 0.93% increase from TL4 to TL6. This means concerning to TL4 with a loading level of 5.3%, a further assembly of nano TiO₂ would have an insignificant effect on the radiative thermal conductivity. This is consistent with the experimental results by Caps et al. [42], which indicated that Al-coating could increase the extinction capacity of polypropylen fibres to a maximum value of ~800 m².kg⁻¹.

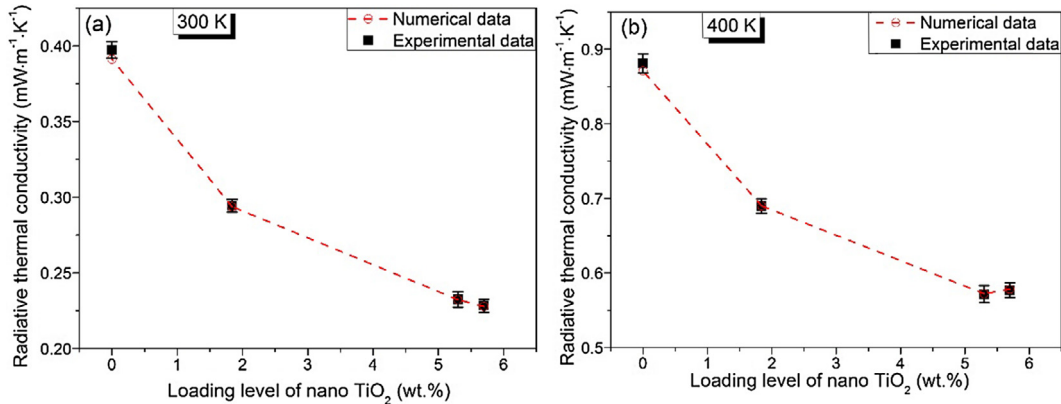


Fig. 9. Comparison of calculated and measured radiative thermal conductivity. (a) 300 K, (b) 400 K.

4.2. Prediction of radiative properties of nano TiO₂ assembled fibrous insulation

Based on the refractive index of nano TiO₂ assembled fibres (Fig. 8(b)), the temperature-dependent effective refractive index of TL0–TL6 could be predicted by Eq. (2), shown in Fig. 10. The effective refractive index ranging in 1.02–1.05 shows an increasing trend with the elevated temperature of 300–400 K. In general, the nano TiO₂ assembled fibres present greater effective refractive index than the pure ones.

Fig. 11(a) shows the experimental extinction coefficients of TL0–TL6 for various wavelengths of 2.5–25 μm , and Fig. 11(b)–(d) shows the numerical ones by Eq. (7). The properties used in the simulations include fibre volume fraction $v_f = 3.0\%$, temperature $T = 300\text{ K}$, diameter $d = 0.5\ \mu\text{m}$ for Fig. 11(b), $d = 1.0\ \mu\text{m}$ for Fig. 11(c) or $d = 2.0\ \mu\text{m}$ for Fig. 11(d). Concerning to experimental diameters the extinction coefficients present the minimum for pure fibres, and increase from TL2 to TL6. The extinction coefficients of $1.0\ \mu\text{m}$ ranging from 50 to $650\ \text{cm}^{-1}$ are remarkably influenced by infrared spectra, which are essentially determined by the intrinsic properties of materials. By comparison analysis, the fluctuation amplitude of extinction coefficients decreases with the increase in the diameter. It could also be deduced by Eq. (7), when bigger diameter turns to smaller extinction coefficient and even smaller fluctuation amplitude. However, the overall extinction coefficient is around $300\ \text{cm}^{-1}$ for both $d = 1.0\ \mu\text{m}$ and $d = 2.0\ \mu\text{m}$.

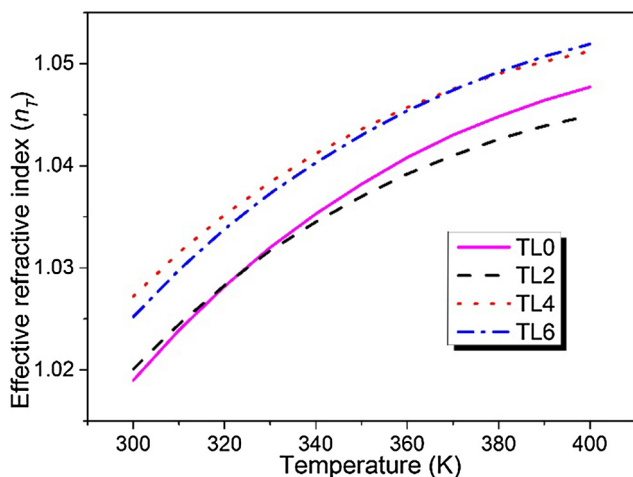


Fig. 10. Predicted temperature-dependent effective refractive index.

Fig. 12 shows the Rosseland mean extinction coefficients of TL0–TL6 for various diameters ranging from 0.3–5.0 μm by Eq. (5). The properties used in the simulations include fibre volume fraction $v_f = 3.0\%$ and temperature $T = 300\text{ K}$ or $T = 400\text{ K}$. A parabola with the opening upward is presented for the Rosseland mean extinction coefficients, which indicates a maximum mean extinction coefficient when the diameter is at the peak value of the parabolic curve (i.e., optimal diameter). The optimal diameter decreases successively with TL0–TL6, although the maximum mean extinction coefficients at 300 and 400 K both range from 250 to $340\ \text{cm}^{-1}$.

Fig. 13 shows the radiative thermal conductivity of TL0–TL6 for various diameters ranging from 0.3 to 5.0 μm by Eq. (1). The properties used in the simulations include fibre volume fraction $v_f = 3.0\%$ and temperature $T = 300\text{ K}$ or $T = 400\text{ K}$. The radiative thermal conductivity at 300 K ranges from $0.22\text{--}0.43\ \text{mW}\cdot\text{m}^{-1}\cdot\text{K}^{-1}$, while it ranges from $0.56\text{--}1.12\ \text{mW}\cdot\text{m}^{-1}\cdot\text{K}^{-1}$ at 400 K. A parabola with the opening downward is presented for the radiative thermal conductivity, which indicates minimum radiative thermal conductivity at the optimal diameter.

4.3. Optimization of radiative thermal conductivity of nano TiO₂ assembled fibrous insulation

Based on the influence of diameter on the radiative thermal conductivity, the diameter is optimized to obtain the optimal diameter and minimum radiative thermal conductivity of TL0–TL6 for various temperatures, as shown in Fig. 14(a) and (b) respectively. The property used in the simulations is fibre volume fraction $v_f = 3.0\%$.

With the increase in the temperature, the optimal diameter decreases while the minimum radiative thermal conductivity increases. The optimal diameters of TL0–TL6 are 2.0, 1.5, 1.1 and $1.0\ \mu\text{m}$ at 300 K, and decrease to about 1.7, 1.2, 0.9 and $0.9\ \mu\text{m}$ at 400 K. The decrease trend is similar to that of fused silica fibres [32], with an optimal diameter dropping from $8.3\ \mu\text{m}$ at 300 K to $3.1\ \mu\text{m}$ at 1000 K. This is mainly due to a decrease in the peak wavelength with an elevated temperature [37]. It can be seen from Fig. 14(a) that the optimal diameter of nano TiO₂ assembled fibres was $0.9\text{--}1.0\ \mu\text{m}$, which is nearly twice smaller than that of pure ones (i.e., $1.7\text{--}2.0\ \mu\text{m}$). It indicates that the optimal diameter of PVDF fibres could be obtained in the nano scale through assembling nano TiO₂.

Fig. 14(b) shows that the minimum thermal conductivities of TL0–TL6 are increased from a range of $0.22\text{--}0.3\ \text{mW}\cdot\text{m}^{-1}\cdot\text{K}^{-1}$ at 300 K to $0.55\text{--}0.73\ \text{mW}\cdot\text{m}^{-1}\cdot\text{K}^{-1}$ at 400 K. Note that the minimum radiative thermal conductivities of TL4 and TL6 are approximately

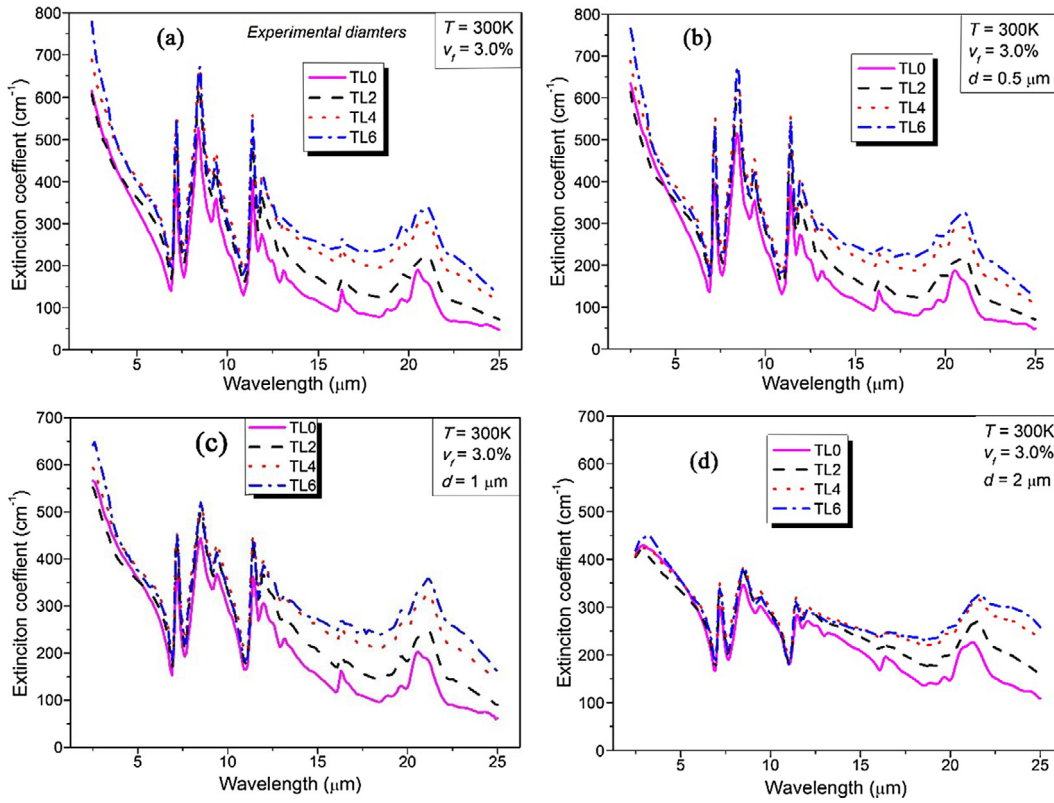


Fig. 11. Predicted infrared spectral extinction coefficient. (a) Experimental diameter, (b) 0.5 μm, (c) 1.0 μm, (d) 2.0 μm.

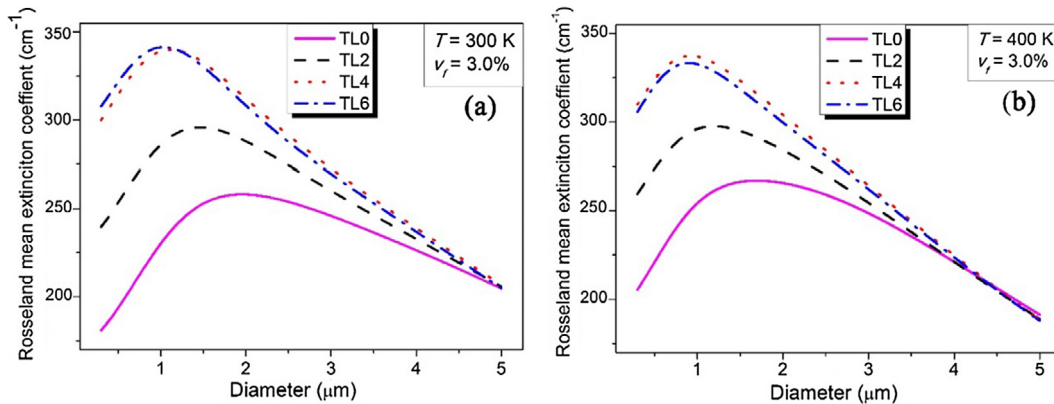


Fig. 12. Rosseland mean extinction coefficient for various diameters. (a) 300 K, (b) 400 K.

equal, rising from $0.22 \text{ mW}\cdot\text{m}^{-1}\cdot\text{K}^{-1}$ at 300 K to $0.55 \text{ mW}\cdot\text{m}^{-1}\cdot\text{K}^{-1}$ at 400 K. This is consistent with the indication from Fig. 9(b), which shows that a further assembling of nano TiO_2 has an insignificant effect on the thermal conductivity after a loading level of 5.3 wt.% (TL4).

To evaluate the enhancement of radiative thermal insulation of fibrous insulations through assembling nano TiO_2 and/or optimizing diameter, two reduction percentages of radiative thermal conductivity are introduced: P_{k1} for the reduction percentages of assembling nano TiO_2 , and P_{k2} for the reduction percentages of optimizing diameter. They are determined by

$$P_{k1} = \frac{k_{r,e}(\text{TLs}) - k_{r,e}(\text{TL0})}{k_{r,e}(\text{TL0})} \times 100\%, \quad (s = 2, 4, 6) \quad (23)$$

$$P_{k2} = \frac{k_{r,e} - k_{r,op}}{k_{r,e}} \times 100\% \quad (24)$$

where subscript *e* indicates the experimental value and *op* indicates the optimal value.

Fig. 15(a) shows P_{k1} for various loading levels at 300 and 400 K by Eq. (23). It can be observed that with the increase in the loading level, the reduction percentage of radiative thermal conductivity increases. For instance, these percentages are 26%, 42% and 43% at 300 K, a slight greater than 22%, 35% and 35% at 400 K, at loading levels of 1.84%, 5.30% and 5.7% respectively. Note that through assembling nano TiO_2 , a 43% reduction in the radiative thermal conductivity is remarkable, when compared with a reduction by some other opacifiers. For instance, carbon opacifiers [43] were reported to obtain a 33% reduction in the radiative thermal conductivity of porous media. A direct addition of nano TiO_2 into a homogeneous matrix also contributed to only 20% enhancement in shielding the radiative performance [44]. It seems that compositing nano TiO_2 using assembly technique could obtain a greater reduction than that by direct addition of nano TiO_2 . This

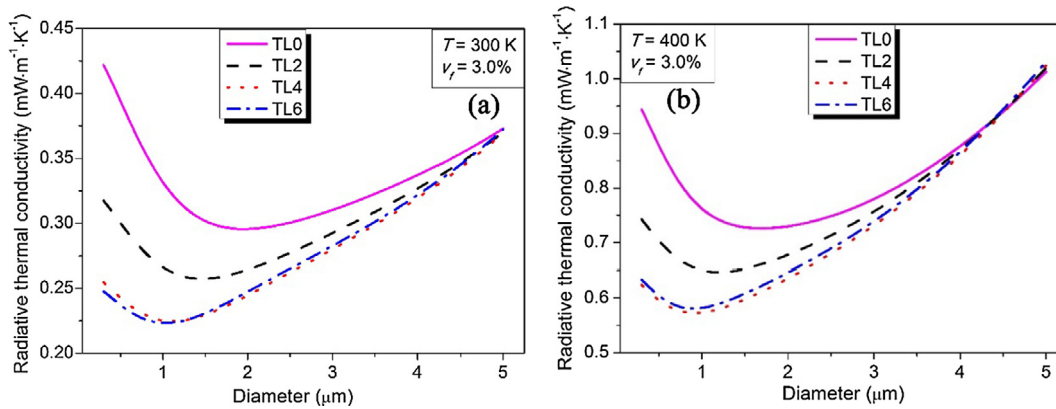


Fig. 13. Radiative thermal conductivity for various diameters. (a) 300 K, (b) 400 K.

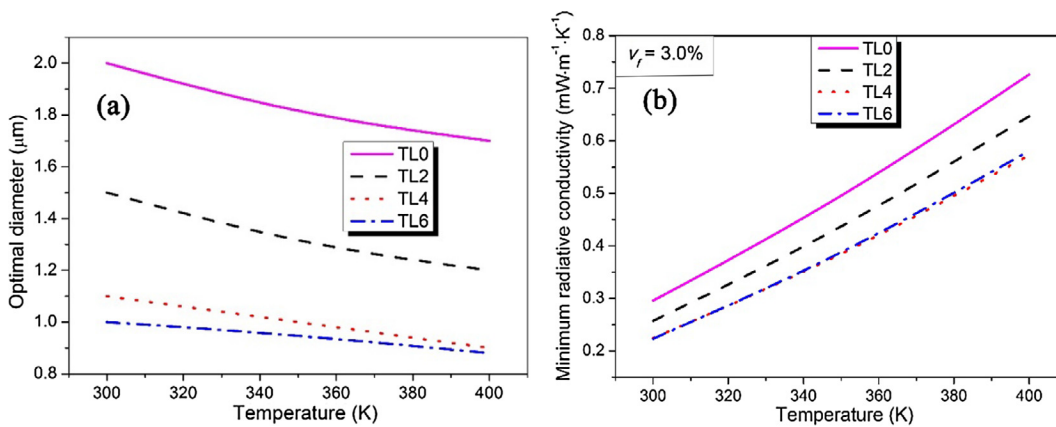


Fig. 14. Optimized results for various temperatures. (a) Optimal diameter, (b) minimum radiative conductivity.

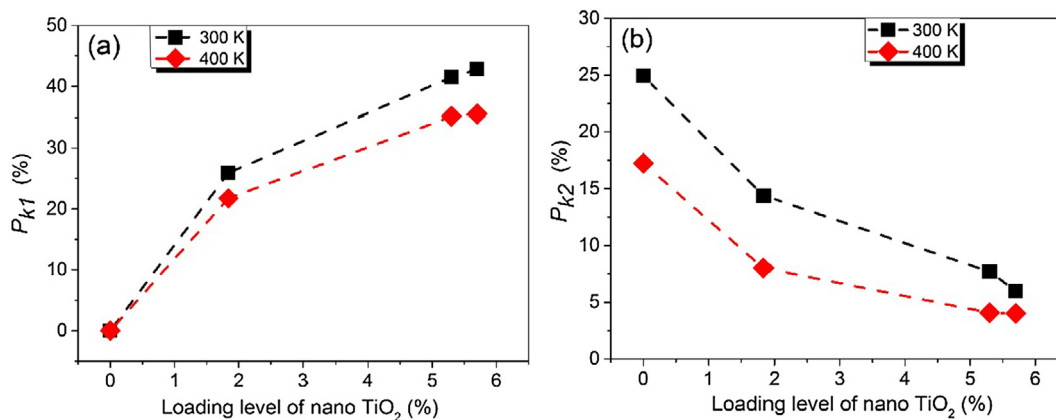


Fig. 15. Reduction percentage of radiative thermal conductivity of fibres and TiO_2 assembled ones. (a) P_{k1} , (b) P_{k2} .

is because the internal scattering radiation in the TiO_2 layer contributes to an increment of the extinction capacity.

It should be noted that the reductions in radiative performance were approximately equal for loading levels of 5.3% (TL4) and 5.7% (TL6). This indicates that a maximum reduction of radiative performance could be obtained at a loading level of 5.3%. Therefore, assembly of nano TiO_2 with a thickness of $\sim 60\text{ nm}$ seems to be sufficient to enhance the shielding radiative performance of PVDF fibres. A similar result was obtained by Caps et al. [42], which indicated that a coating thickness of $\sim 80\text{ nm}$ Al opacifiers could be used to cover the polypropylen microfibre effectively.

Fig. 15(b) shows P_{k2} for various loading levels at 300 and 400 K by Eq. (24). With the increase in the loading level of nano TiO_2 , the reduction percentage of radiative thermal conductivity by optimizing fibre diameter decreases. For instance, from TL0 to TL6 these percentages decrease from 25% to 6% at 300 K, while from 17% to 4% at 400 K. This is because with the increase in the loading level, the difference between the experimental diameter and the optimal diameter decreases. For instance at 300 K, the experimental diameter and the optimal diameter of TL0 are 0.52 and $2.0\ \mu\text{m}$, while those of TL6 are 0.582 and $0.9\ \mu\text{m}$ respectively. Apparently the diameter difference of TL6 is much smaller than that of TL0.

This would contribute a smaller reduction in the radiative thermal conductivity with the increase in the loading level [3].

5. Conclusions

A numerical model was presented for the predictions of radiative thermal properties of nano TiO₂ assembled fibrous insulations. To ensure the validation of the numerical model and to provide the fundamental parameters, nano TiO₂ assembled fibrous insulations with different TiO₂ loading levels were experimentally prepared and characterized. The effects of TiO₂ loading level and fibre diameter on radiative thermal properties were analysed to investigate the mechanism of radiative thermal transfer of nano TiO₂ assembled insulations. The radiative thermal conductivity could be decreased by assembling nano TiO₂ and/or optimizing diameters. The nano TiO₂ led to a significant enhancement of radiative thermal insulation for fibrous insulations, i.e., an almost 43% reduction of radiative thermal conductivity. A further 6% decrease of radiative thermal conductivity could be obtained by optimizing the diameter. By introducing nano TiO₂, the optimal fibre diameter could be reduced from 1.7–2.0 μm to 0.9–1.0 μm, which indicated that the optimal fibre diameter in the experimental scope (i.e. 0.2–1.0 μm) could be achieved through assembling nano TiO₂.

Acknowledgements

This research was supported by the National Natural Science Foundation of China (No. 51678167), the Guangdong Province Natural Science Foundation for Distinguished Young Scientists of China (No. S2013050014139) and the Major research project of Guangdong Provincial Department of Education (No. 2016KZDXM035).

Conflict of interest

The authors declared that there is no conflict of interest.

References

- [1] L.F. Liu, H.Q. Li, A. Lazzaretto, G. Manente, C.Y. Tong, Q.B. Liu, N.P. Li, The development history and prospects of biomass-based insulation materials for buildings, *Renew. Sust. Energy Rev.* 69 (2017) 912–932.
- [2] Y. Si, J.Y. Yu, X.M. Tang, J.L. Ge, B. Ding, Ultralight nanofibre-assembled cellular aerogels with superelasticity and multifunctionality, *Nat. Commun.* 5802 (2014) 1–9.
- [3] J.M. Yang, H.J. Wu, M.R. Wang, S.Q. He, H.K. Huang, Prediction and optimization of radiative thermal properties of ultrafine fibrous insulations, *Appl. Therm. Eng.* 104 (2016) 394–402.
- [4] Y. Dauvois, D. Rochais, F. Enguehard, J. Taine, Statistical radiative modeling of a porous medium with semi transparent and transparent phases: application to a felt of overlapping fibres, *Int. J. Heat Mass Transf.* 106 (2017) 601–618.
- [5] W. Feng, M. Qin, Y.Y. Feng, Toward highly thermally conductive all-carbon composites: structure control, *Carbon* 109 (2016) 575–597.
- [6] M.R. Wang, N. Pan, Modeling and prediction of the effective thermal conductivity of random open-cell porous foams, *Int. J. Heat Mass Transf.* 51 (2008) 1325–1331.
- [7] G. Bastos, F. Patino-barbeito, F. Patino-cambeiro, J. Armesto, Admixtures in cement-matrix composites for mechanical reinforcement, sustainability, and smart features, *Materials* 972 (2016) 1–27.
- [8] M.R. Wang, N. Pan, Predictions of effective physical properties of complex multiphase materials, *Mater. Sci. Eng. R-Rep* 63 (2008) 1–30.
- [9] W.Q. Li, Z.G. Qu, Experimental study of effective thermal conductivity of stainless steel fiber felt, *Appl. Therm. Eng.* 86 (2015) 119–126.
- [10] M. Alam, H. Singh, S. Suresh, D.A.G. Redpath, Energy and economic analysis of Vacuum Insulation Panels (VIPs) used in non-domestic buildings, *Appl. Energy* 188 (2017) 1–8.
- [11] T. Xie, Y.L. He, Heat transfer characteristics of silica aerogel composite materials: structure reconstruction and numerical modeling, *Int. J. Heat Mass Transf.* 95 (2016) 621–635.
- [12] D. He, Y.L. Li, I.S. Wang, J.S. Wu, Y.L. Yang, Q. An, Carbon wrapped and doped TiO₂ mesoporous nanostructure with efficient visible-light photocatalysis for NO removal, *Appl. Surf. Sci.* 391 (2017) 318–325.
- [13] M. Sabet, H. Jahangiri, E. Ghashghaei, Improving microwave absorption of the polyaniline by carbon nanotube and needle-like magnetic nanostructures, *Synth. Met.* 224 (2017) 18–26.
- [14] L. Xu, Y.G. Jiang, J.Z. Feng, J. Feng, C.W. Yue, Infrared-opacified Al₂O₃-SiO₂ aerogel composites reinforced by SiC-coated mullite fibers for thermal insulations, *Ceram. Int.* 41 (2015) 437–442.
- [15] M. Foruzanmehr, L. Boulos, P.Y. Vuillaume, S. Elkoun, M. Robert, The effect of cellulose oxidation on interfacial bonding of nano-TiO₂ coating to flax fibers, *Cellulose* 24 (2017) 1529–1542.
- [16] P.T. Zhao, J.T. Fan, Electrospun nylon 6 fibrous membrane coated with rice-like TiO₂ nanoparticles by an ultrasonic-assistance method, *J. Membr. Sci.* 355 (2010) 91–97.
- [17] H.J. Wu, J.T. Fan, X.H. Qin, G.G. Zhang, Thermal radiative properties of electrospun superfine fibrous PVA films, *Mater. Lett.* 62 (2008) 828–831.
- [18] G.Q. Zu, J. Shen, W.Q. Wang, L.P. Zou, Y. Lian, Z.H. Zhang, B. Liu, F. Zhang, Robust, highly thermally stable, core-shell nanostructured metal oxide aerogels as high-temperature thermal superinsulators, adsorbents, and catalysts, *Chem. Mater.* 26 (2014) 5761–5772.
- [19] N. Nouri, F. Panerai, K.A. Tagavi, N.N. Mansour, A. Martin, Evaluation of the anisotropic radiative conductivity of a low-density carbon fiber material from realistic microscale imaging, *Int. J. Heat Mass Transf.* 95 (2016) 535–539.
- [20] X.F. Wang, J.T. Fan, Heat transfer through fibrous assemblies incorporating reflective interlayers, *Int. J. Heat Mass Transf.* 55 (2012) 8032–8037.
- [21] N.L. Mckay, T. Timusk, B. Farnworth, Determination of optical properties of fibrous thermal insulation, *J. Appl. Phys.* 55 (1984) 4064–4071.
- [22] P.W. Gibson, C. Lee, F. Ko, D. Reneker, Application of nanofiber technology to nonwoven thermal insulation, *J. Eng. Fiber Fabr.* 2 (2007) 32–40.
- [23] M.A. Tahir, H.V. Tafreshi, S.A. Hosseini, B. Pourdeyhimi, Modeling the role of microstructural parameters in radiative heat transfer through disordered fibrous media, *Int. J. Heat Mass Transf.* 53 (2010) 4629–4637.
- [24] T. Tong, C. Tien, Radiative heat transfer in fibrous insulations—Part I: analytical study, *J. Heat Transf.* 105 (1983) 70–75.
- [25] R. Arambakam, H.V. Tafreshi, B. Pourdeyhimi, Dual-scale 3-D approach for modeling radiative heat transfer in fibrous insulations, *Int. J. Heat Mass Transf.* 64 (2013) 1109–1117.
- [26] R. Arambakam, H.V. Tafreshi, B. Pourdeyhimi, Modeling performance of multi-component fibrous insulations against conductive and radiative heat transfer, *Int. J. Heat Mass Transf.* 71 (2014) 341–348.
- [27] G. Mie, Beiträge zur Optik trüber Medien, speziell kolloidaler Metallösungen, *Annalen Der Physik* 330 (1908) 377–445.
- [28] R.D.L. Kronig, On the theory of dispersion of x-rays, *Josa* 12 (1926) 547–556.
- [29] M.F. Modest, *Radiative Heat Transfer*, Academic Press, New York, 2013.
- [30] S.K. Padmanabhan, E.U. Haq, A. Licciulli, Synthesis of silica cryogel-glass fiber blanket by vacuum drying, *Ceram. Int.* 42 (2016) 7216–7222.
- [31] T. Xie, Y.L. He, Z.J. Hu, Theoretical study on thermal conductivities of silica aerogel composite insulating material, *Int. J. Heat Mass Transf.* 58 (2013) 540–552.
- [32] J.M. Yang, H.J. Wu, S.Q. He, M.R. Wang, Prediction of thermal conductivity of fiber/aerogel composites for optimal thermal insulation, *J. Porous Media* 18 (2015) 971–984.
- [33] R. Siegel, *Thermal Radiation Heat Transfer*, CRC Press, Florida, 2001.
- [34] G.R. Cunningham, S.C. Lee, Radiative properties of fibrous insulations – theory versus experiment, *J. Thermophys. Heat Transf.* 10 (1996) 460–466.
- [35] C.F. Bohren, D.R. Huffman, *Absorption and Scattering of Light by Small Particles*, Wiley, New York, 2008.
- [36] E.D. Palik, *Handbook of Optical Constants of Solids*, Academic Press, San Diego, 1998.
- [37] M. Planck, On the law of distribution of energy in the normal spectrum, *Ann. Phys.* 4 (1901) 553–558.
- [38] Beer, Bestimmung der Absorption des rothen Lichts in farbigen Flüssigkeiten (Determination of the absorption of red light in colored liquids), *Annalen der Physik und Chemie* 86 (1852) 78–88.
- [39] L.M. Ruan, X.Y. Wang, H. Qi, S.G. Wang, Experimental investigation on optical constants of aerosol particles, *J. Aerosol. Sci.* 42 (2011) 759–770.
- [40] M.E. Milham, R.H. Frickel, J.F. Embury, D.H. Anderson, Determination of optical constants from extinction measurements, *J. Opt. Soc. Am.* 71 (1981) 1099–1106.
- [41] J.A. Lee, K.C. Krogman, M.L. Ma, R.M. Hill, P.T. Hammond, G.C. Rutledge, highly reactive multilayer-assembled TiO₂ coating on electrospun polymer nanofibers, *Adv. Mater.* 21 (2009) 1252–1256.
- [42] R. Caps, M.C. Arduini-Schuster, H.P. Ebert, J. Fricke, Improved thermal radiation extinction in metal coated polypropylen microfibers, *Int. J. Heat Mass Transf.* 36 (1993) 2789–2794.
- [43] S.Q. Zeng, A. Hunt, R. Greif, Theoretical modeling of carbon content to minimize heat transfer in silica aerogel, *J. Non-Cryst. Solids* 186 (1995) 271–277.
- [44] J. Wang, Monolithic silica aerogel insulation doped with TiO₂ powder and ceramic fibers, *J. Non-Cryst. Solids* 186 (1995) 296–300.